Dimensionality-Driven Metal-Insulator Transition in Spin-Orbit-Coupled $SrIrO_3$

P. Schütz,[1] D. Di Sante,[2] L. Dudy,[1] J. Gabel,[1] M. Stübinger,[1] M. Kamp,[1] Y. Huang,[3] M. Capone,[4] M.-A. Husanu,[5,6] V. N. Strocov,[6] G. Sangiovanni,[2] M. Sing,[1] and R. Claessen[1]

[1]*Physikalisches Institut and Röntgen Center for Complex Material Systems (RCCM), Universität Würzburg, Am Hubland, D-97074 Würzburg, Germany*

[2]*Institut für Theoretische Physik und Astrophysik, Universität Würzburg, Am Hubland, D-97074 Würzburg, Germany*

[3]*Van der Waals—Zeeman Insitute, University of Amsterdam, Science Park 904, 1098 XH Amsterdam, The Netherlands*

[4]*CNR-IOM-Democritos National Simulation Centre and International School for Advanced Studies (SISSA), Via Bonomea 265, I-34136 Trieste, Italy*

[5]*National Institute of Materials Physics, Atomistilor 405 A, 077125 Magurele, Romania*

[6]*Swiss Light Source, Paul Scherrer Institut, CH-5232 Villigen, Switzerland*

(Received 29 June 2017; published 22 December 2017)

Upon reduction of the film thickness we observe a metal-insulator transition in epitaxially stabilized, spin-orbit-coupled $SrIrO_3$ ultrathin films. By comparison of the experimental electronic dispersions with density functional theory at various levels of complexity we identify the leading microscopic mechanisms, i.e., a dimensionality-induced readjustment of octahedral rotations, magnetism, and electronic correlations. The astonishing resemblance of the band structure in the two-dimensional limit to that of bulk Sr_2IrO_4 opens new avenues to unconventional superconductivity by "clean" electron doping through electric field gating.

DOI: 10.1103/PhysRevLett.119.256404

Although typically viewed as disparate properties, the interplay between strong spin-orbit coupling (SOC) and electronic correlations in high-Z 5d transition metal oxides can lead to exotic quantum states of matter like Kitaev spin liquids [1,2] and topological phases [3,4]. A prominent example is the Mott-insulating state found in the prototypical system Sr_2IrO_4 [5], which is promoted by the lifted orbital degeneracy of the t_{2g} manifold due to the entanglement of orbital and spin degrees of freedom in the presence of strong SOC [1]. Its quasi-two-dimensional (2D) layered-perovskite structure with corner-shared IrO_6 octahedra hosts a square lattice of antiferromagnetically coupled $J_{\mathrm{eff}} = 1/2$ pseudospins reminiscent of the high-T_C superconducting cuprate parent materials [6]. Indeed, Sr_2IrO_4 is considered a promising candidate for exotic superconductivity since it reproduces much of the fermiology of hole-doped cuprates upon electron doping [7,8].

The strontium iridate Ruddlesden-Popper (RP) compounds $Sr_{n+1}Ir_nO_{3n+1} = ([SrIrO_3]_n, SrO)$ essentially consist of n $SrIrO_3$ perovskite layers, intercalated by SrO layers and laterally shifted against each other such that no Ir—O—Ir bonds persist between neighboring $[SrIrO_3]_n$ blocks [9]. As one veers away from the quasi-2D limit (Sr_2IrO_4, $n = 1$) the Mott-insulating state breaks down as evidenced by the narrow-gap bilayer system $Sr_3Ir_2O_7$ hosting a collinear antiferromagnetic order [10,11] and the three-dimensional ($n = \infty$) semimetallic $SrIrO_3$[12]. However, the instability of bulk $Sr_{n+1}Ir_nO_{3n+1}$ for $n > 2$ impedes a systematic investigation of the dimensionality-induced metal-insulator-transition (MIT). In an attempt to mimic the layered RP structure, a concurrent metal-insulator and magnetic transition has been observed in artificially tailored $([SrIrO_3]_m, SrTiO_3)$ superlattices, where the intercalated SrO layers were substituted with $SrTiO_3$ monolayers [13]. Noticeably, the different magnetic orders found in the bilayer analogues reflect the persisting non-negligible coupling between neighboring bilayers across the $SrO/SrTiO_3$ blocking layers. Indeed, both magnetism and resistivity have recently been shown to be affected by pronounced interlayer coupling in $(SrIrO_3, [SrTiO_3]_k)$ superlattices [14].

In this Letter, we investigate the electronic and structural properties of epitaxially grown ultrathin perovskite $SrIrO_3$ films, which represent a considerably cleaner (or: better defined) approach to the two-dimensional limit than the superlattices. We observe the opening of a distinct charge gap at the chemical potential and concurrent changes in the film crystalline structure as a function of the film thickness. In a combined experimental and theoretical approach using soft-x-ray angle-resolved photoelectron spectroscopy (SX ARPES) and *ab initio* density functional theory (DFT and DFT + U) calculations we investigate the evolution of the electronic band structure across the film thickness-driven MIT. We thereby elucidate the complex, microsopic interplay between electronic correlations, structural degrees of freedom, magnetism, and dimensionality.

$SrIrO_3$ thin films were heteroepitaxially grown on TiO_2-terminated $SrTiO_3$ (001) substrates by pulsed laser deposition (PLD) from a polycrystalline $SrIrO_3$ target. The films adopt a pseudotetragonal perovskite structure with an in-plane lattice constant locked to that of $SrTiO_3$ ($a = 3.905$ Å) and an out-of-plane lattice constant of

3.99 Å. Because of collective rotations of the IrO_6 octahedra ($a^+b^-b^-$ in Glazer notation with the a axis along the [100] or [010] direction of the substrate [15,16]) the real-space unit cell is enlarged by $2 \times \sqrt{2} \times \sqrt{2}$ with respect to the tetragonal unit cell (for a thorough structural characterization, see the Supplemental Material [17]). SX-ARPES measurements were performed at 20 K at the ADRESS beam line of the Swiss Light Source, Paul Scherrer Institute [26,27]. Density functional theory calculations were performed by using the VASP *ab initio* simulation package [28] within the projector-augmented-plane-wave (PAW) method [29,30], using the generalized gradient approximation (GGA) as parametrized by the Perdew-Burke-Ernzerhof GGA functional [31]. Spin-orbit coupling was self-consistently included [32] and the Coulomb repulsion U and exchange interaction J of Ir d orbitals were treated within the rotationally invariant DFT + U scheme of Liechtenstein, Anisimov, and Zaanen [33].

Figure 1 shows the experimental and theoretical band structures obtained from SX ARPES on a 9-unit-cell- (u.c.) thick metallic $SrIrO_3$ film and paramagnetic DFT($+U$) calculations for the bulk material. As the starting point for the analysis of the photoemission data we consider a simplified tetragonal perovskite structure compressively strained to the $SrTiO_3$ substrate ($a_\perp/a_{STO} \approx 1.02$) as depicted in Figs. 1(a) and 1(b). We investigate the combined effect of on-site Coulomb repulsion U and exchange-coupling J on the DFT($+U$) band structure and Fermi surface topology. The resulting bands are projected onto a $J_{\text{eff}} = (1/2, 3/2)$ basis [1]. As seen in Figs. 1(c) and 1(e) DFT calculations already capture some of the low-energy spectral features. However, most noteworthy, they predict an Ir $5d\,e_g$ electron pocket around Γ and an Ir $J_{\text{eff}} = 3/2$ hole pocket around the A point, which are not seen in experiment. A way to reduce the discrepancy is to include short range Coulomb repulsion. Rather than looking for the lowest-energy solution within DFT + U, which would be a magnetic insulator at variance with experiment, we discard magnetism for this 9 u.c. film. In this framework, U mainly acts to shift orbitals with different occupations relative to each other. We chose its value to match the position of the ARPES bands [17], thereby pushing the bands either above or below the chemical potential, whereupon the e_g electrons are being predominantly transferred into the $J_{\text{eff}} = 3/2$ band, leaving the $J_{\text{eff}} = 1/2$ Luttinger volume relatively unchanged. It does not come as a surprise that the resulting values of U (3.4) and J (0.4 eV) are significantly larger than *ab initio* estimates using the constraint random phase approximation (cRPA) [35,36]. A more accurate treatment of the many-body processes based on dynamical mean field theory (DMFT) would most likely account for the experimental features with smaller values of the interaction (for DMFT studies for Sr_2IrO_4 see Refs. [37,38]).

Despite the overall good agreement, a closer inspection of the DFT + U band structure reveals subtle differences to the experimental data. In particular, the narrow band at the chemical potential between the X and M point and the spectral weight near the R point are not captured in the DFT + U calculations in Fig. 1(d). Indeed, previous ARPES studies using ultraviolet light have reported such narrow bands as a result of backfolding due to octahedral rotations [16], which introduce a periodic perturbation of

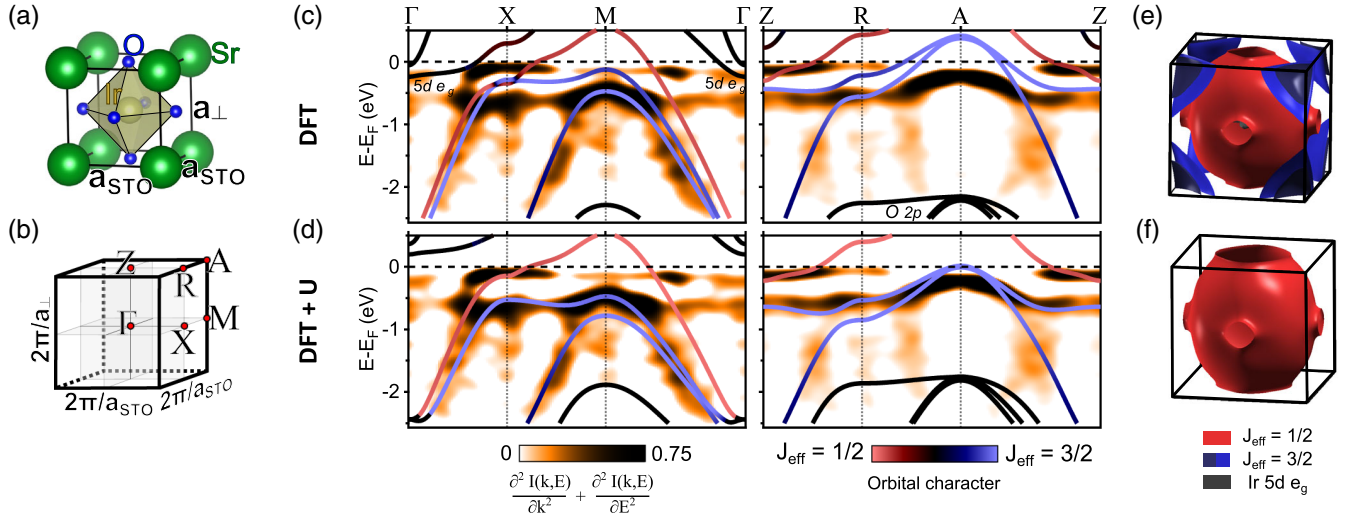

FIG. 1. (a) Real and (b) reciprocal space structure of strained, tetragonal $SrIrO_3$ without octahedral rotations [34]. (c),(d) E vs k dispersions along the high-symmetry lines $\Gamma - X - M - \Gamma$ and $Z - R - A - Z$ measured by SX ARPES ($h\nu = 745$ eV and $h\nu = 660$ eV, respectively) and compared to DFT + U calculations. The band structure was calculated for the tetragonal setting and projected onto a $J_{\text{eff}} = (1/2, 3/2)$ basis with (c) $U = 0$ and $J = 0$ eV and (d) $U = 3.4$ and $J = 0.4$ eV. The introduction of a sizable on-site Coulomb repulsion significantly enhances the agreement between theory and experimental results. (e),(f) Fermi surface topology without (e) and with (f) on-site Coulomb repulsion U and exchange coupling J.

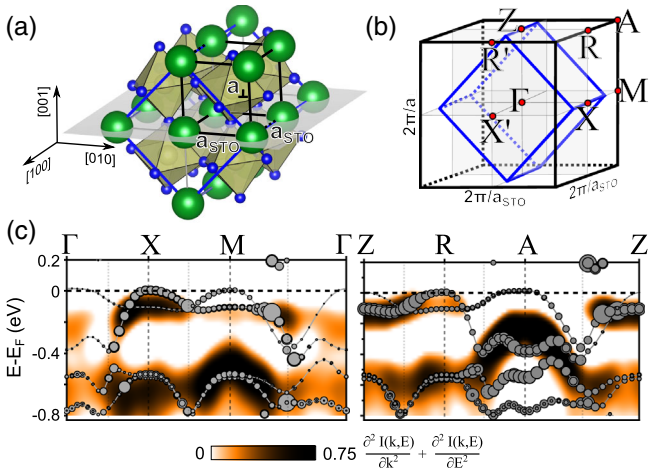

FIG. 2. (a) Real-space lattice structure of $SrIrO_3$ including octahedral rotations ($a^+b^-b^-$ in Glazer notation with the a axis orthogonal to the film surface normal) and strain. The orthorhombic unit cell (blue) is enlarged by $2 \times \sqrt{2} \times \sqrt{2}$ with respect to the tetragonal unit cell (black). (b) Reciprocal space structure of the orthorhombic (blue) and tetragonal (black) structure. (c) SX-ARPES band maps along the pseudotetragonal high-symmetry lines $\Gamma - X - M - \Gamma$ and $Z - R - A - Z$ in comparison to DFT + U band structure calculated in the orthorhombic setting and unfolded into the tetragonal Brillouin zone.

the crystal potential that enlarges (reduces) the real-space unit cell (Brillouin zone) as depicted in Figs. 2(a) and 2(b). In Fig. 2(c) we present the corresponding band structure unfolded into the original Brillouin zone, thereby taking into account the effect of this weak symmetry breaking by calculating the proper spectral weight distribution as described in Ref. [39] (represented by the size of the gray dots). The weighted, unfolded bands have a narrow bandwidth of ≈400 meV and resolve the aforementioned discrepancies between experiment and theory by exhibiting Fermi crossings around the X and R point. Note that the seemingly more pronounced backfolded band structure in ARPES measurements using He I light [16,40] may be due to different matrix elements and/or the inherently higher surface sensitivity as compared to photoemission in the soft-x-ray regime [41,42].

Epitaxially stabilized $SrIrO_3$ thin films essentially exhibit bulk electronic and structural properties above a thickness of at least 9 u.c., i.e., paramagnetism and metallicity with a partially filled $J_{\mathrm{eff}} = 1/2$ band. Figure 3(a) shows photoemission spectra (He I, $h\nu = 21.2$ eV) of $SrIrO_3$ films of smaller thicknesses with $m = 4$, 3, 2, 1, and 0 u.c. (bare $Nb:SrTiO_3$). As expected in the three-dimensional limit thick films ($m \geq 4$) exhibit a metallic density of states with a pronounced Fermi-Dirac cutoff at the chemical potential. Intriguingly, at $m = 3$ the Fermi cutoff disappears and upon further reduction of the film thickness a distinct charge gap opens. Hence, in analogy to the RP iridates the films undergo a MIT transition as a function of dimensionality as also observed in transport measurements [43]. As shown in the inset of Fig. 3(a) magnetic DFT + U calculations for m $SrIrO_3$ layers on 4 $SrTiO_3$ layers (denoted by $m/\!/4$) similarly show a decreasing charge gap in the k-integrated density of states (DOS) as m is increased. Note, however, that in the presence of magnetic ordering the increasing film thickness alone does not trigger a transition from insulating to metallic in our calculations.

The photoemission gap opening is accompanied by a structural transition as inferred from low energy (LEED) and reflection high-energy electron diffraction (RHEED) from the film surface. As seen in Fig. 3(b), the surface periodicity, which reflects the complex rotational pattern of

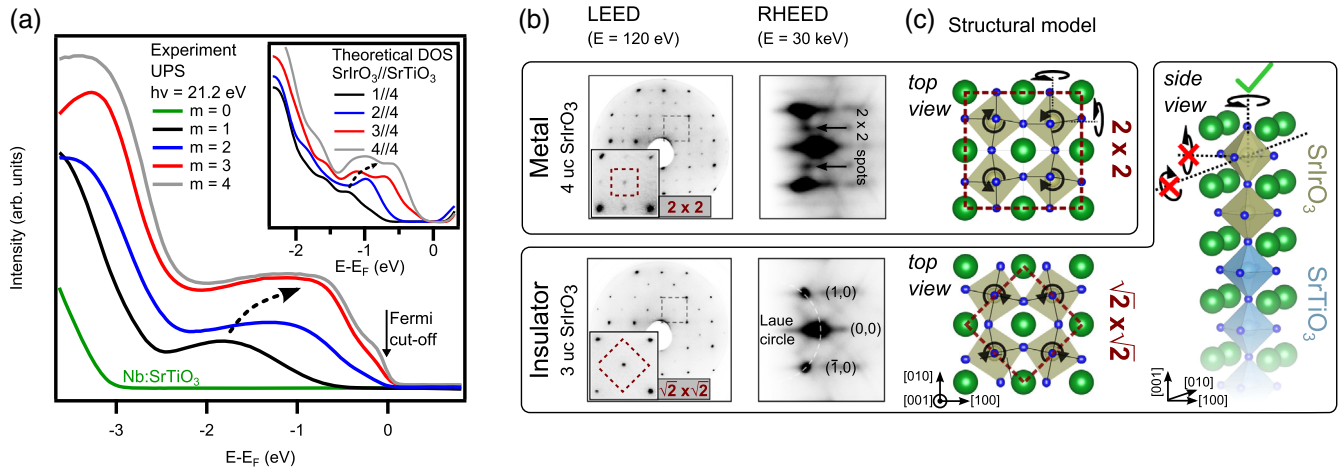

FIG. 3. (a) Ultraviolet photoelectron spectroscopy (UPS) of $SrIrO_3$ films with thickness m (bare $Nb:SrTiO_3$, $m = 1, 2, 3, 4$ u.c.) exhibiting the opening of a charge gap between 3 and 4 u.c. Inset: DOS from DFT + U slab calculations of m $SrIrO_3$ layers on 4 $SrTiO_3$ layers ($m/\!/4$). (b) LEED and RHEED patterns of an insulating ($m = 3$) and a metallic ($m = 4$) $SrIrO_3$ film exhibit a structural transition from a $\sqrt{2} \times \sqrt{2}$ to a 2×2 surface periodicity across the MIT. (c) Structural model explaining the observed changes as result of suppressed in-plane octahedral rotations in thin films ($a^0a^0b^{+/-}$) as opposed to the bulk rotational pattern ($a^+b^-b^-$) observed in thick films.

IrO_6 octahedra within the film, changes at the threshold thickness. In atomically thin, insulating films only rotations about the surface normal prevail, whereas rotations about the in-plane directions are suppressed due to the corner-shared octahedral network between $SrIrO_3$ and the $SrTiO_3$ substrate [Fig. 3(c)], which is a cubic perovskite without octahedral rotations at room temperature. Analogously, the nonmetallic RP iridates Sr_2IrO_4 and $Sr_3Ir_2O_7$ exclusively exhibit octahedral rotations about the c axis (reducing their space group symmetry from $I4/mmm$ to $I4_1/acd$ and $Bbcb$, respectively) [11,44–46].

Figure 4(a) shows the SX-ARPES band map of a 1 u.c. $SrIrO_3$ film grown on $Nb:SrTiO_3$ in comparison to the DFT + U band structure of a $1/\!/4$ $SrIrO_3/\!/SrTiO_3$ slab. In excellent agreement with each other the experimental and theoretical data exhibit weakly dispersing bands with a valence band maximum at the M point. Interestingly, as seen in the k-integrated DOS of the $1/\!/4$ slab in Fig. 4(b), only the antiferromagnetic DFT + U ground state is insulating, whereas the paramagnetic solution remains metallic as in the three-dimensional limit. This finding is in line with the enhanced spin fluctuations near the thickness-driven MIT recently observed in magnetoconductance measurements of samples identical to ours [43]. The DFT + U ground state is characterized by in-plane magnetic moments which are aligned antiferromagnetically, with a weak ferromagnetic component ($\approx 0.03\ \mu_B$/Ir) resulting from octahedral rotations via a Dzyaloshinskii-Moriya interaction as depicted in Fig. 4(b). The dimensionality-induced MITs observed in RP iridate crystals [1,11,47–49] and $[(SrIrO_3)_m, SrTiO_3]$ superlattices [13] are similarly accompanied by a magnetic transition and intriguingly, the antiferromagnetic DFT + U band structure of the $1/\!/4$ $SrIrO_3$ slab shows a striking similarity to that of bulk Sr_2IrO_4 shown in Fig. 4(c). Our analysis suggests that the observed gap opening is compatible with a transition from a nonmagnetic to a magnetic ground state in DFT + U. Whether or not this translates into a long range ordering at finite temperatures at the critical thickness and whether an order parameter persists in the two-dimensional limit ($m = 1$) are currently debated open questions [14].

For a deeper understanding of the driving mechanism behind the MIT one needs to take into account the subtle interplay between the dominant, comparably strong physical interactions (U, W, SOC) in 5d transition metal oxides, which leaves the electronic and magnetic ground state highly susceptible to small external perturbations. Here we have demonstrated that the $SrIrO_3$ film thickness can be used as an experimental control parameter to tune three physical properties, which cooperatively determine the system's ground state. First, the effective Coulomb interaction U/W increases upon reduction of m since the coordination of Ir sites becomes smaller, hence providing less hopping channels (smaller W) and less screening (bigger U) [36]. Second, the crystalline structure due to the IrO_6 rotations deviates from the rotational pattern of bulk $SrIrO_3$ in the two-dimensional limit, since the octahedral network with the cubic $SrTiO_3$ substrate imposes constraints upon the in-plane rotations. Finally, the onset of an insulating state is associated with magnetic correlations. The actual stabilization of a long-range ordered magnet is a very delicate issue, due to the sensitivity to the dimensionality and to the competition between in- and out-of-plane coupling [11]. The strong cooperative interplay between these degrees of freedom constitutes the complexity of the system. Specifically, octahedral rotations strongly affect the magnetic coupling in iridates due to pseudodipolar and Dzyaloshinskii-Moriya exchange interactions as evidenced by the locking of the Ir magnetic moments to the rotated oxygen octahedra [48]. In turn, the symmetry breaking due to octahedral rotations provides further spin-dependent hopping terms in the J_{eff} basis that additionally increase the kinetic energy W [49]. This

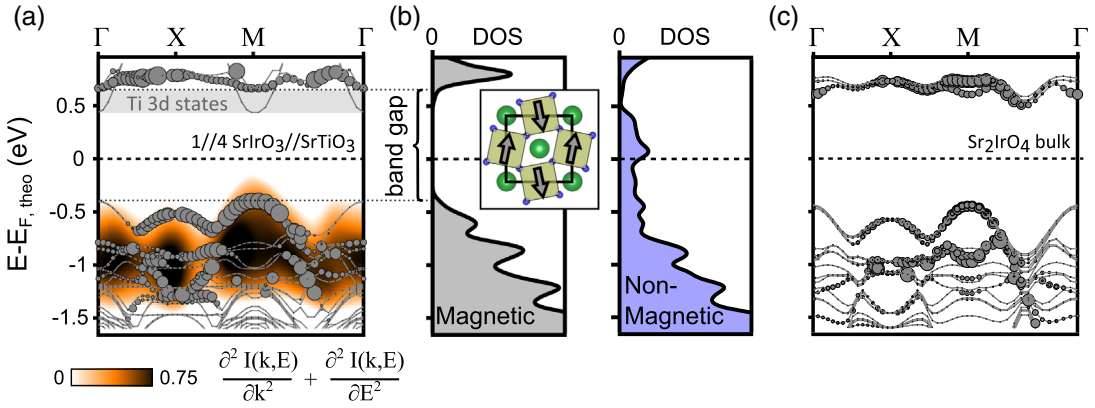

FIG. 4. (a) SX-ARPES band map of a $SrIrO_3$ monolayer grown on $Nb:SrTiO_3$ and DFT + U band structure of a $1/\!/4$ $SrIrO_3/\!/SrTiO_3$ slab along the pseudotetragonal high-symmetry line $\Gamma - X - M - \Gamma$. (b) DFT + U k-integrated density of states (DOS) of the $1/\!/4$ slab. The antiferromagnetic solution exhibits a charge gap of ≈ 1 eV, while the nonmagnetic solution is in a metallic state. (c) DFT + U band structure calculation for bulk Sr_2IrO_4.

tendency is reflected in the (albeit small) resistivity drop at $T = 105$ K [50], where the $SrTiO_3$ substrate undergoes a structural transition involving $a^0a^0c^-$-rotations of the TiO_6 octahedra [51,52], which can induce in-plane tiltings in the $SrIrO_3$ film. On the other hand, changes in U/W will affect the magnetic ordering by altering the required critical on-site Coulomb repulsion U for the transition to an antiferromagnetic ground state [49].

The underlying reason for this extraordinary dimensionality dependence is the spatially three-dimensional $J_{\text{eff}} = 1/2$ Kramers doublet wave function, which results from the mixing of orbitals of different symmetries with the spin degrees of freedom due to the strong spin-orbit coupling in $5d$ systems. This is in stark contrast to typical $3d$ systems like the cuprates, where the planar e_g orbitals host the $S = 1/2$ magnetic moments in the absence of strong spin-orbit coupling. With regard to Sr_2IrO_4 as a potential parent material for exotic superconductivity, the analogy between monolayer $SrIrO_3$ and bulk Sr_2IrO_4 may open a promising experimental avenue towards electron doping without the introduction of disorder through electrostatic or ion-liquid gating, possibly pushing the system into a novel, spin-orbit-driven superconducting phase.

This work was supported by the Deutsche Forschungsgemeinschaft (SFB 1170 *ToCoTronics* and FOR 1162). We thank D. Groenendijk and A. Caviglia (both at TU Delft), and C. Autieri and S. Picozzi (both at CNR-SPIN, L'Aquila) for fruitful discussions, as well as D. Pohl, A. Lubk, T. Gemming, and B. Büchner (IFW Dresden) for transmission electron microscopy measurements. D. D. S. and G. S. gratefully acknowledge the Gauss Centre for Supercomputing e.V. for funding this project by providing computing time on the GCS Supercomputer SuperMUC at Leibniz Supercomputing Centre (LRZ). M. C. acknowledges financial support from MIUR through the PRIN 2015 program (Prot. 2015C5SEJJ001) and SISSA/CNR project Superconductivity, Ferroelectricity, and Magnetism in bad metals. D. D. S acknowledges ERC-StG-336012-Thomale-TOPOLECTRICS. M.-A. H. was supported by the Swiss Excellence Scholarship Grant ESKAS-No. 2015.0257.

[1] G. Jackeli and G. Khaliullin, Phys. Rev. Lett. **102**, 017205 (2009).
[2] W. Witczak-Krempa, G. Chen, Y. B. Kim, and L. Balents, Annu. Rev. Condens. Matter Phys. **5**, 57 (2014).
[3] D. Pesin and L. Balents, Nat. Phys. **6**, 376 (2010).
[4] X. Zhang, H. Zhang, J. Wang, C. Felser, and S.-C. Zhang, Science **335**, 1464 (2012).
[5] B. J. Kim, H. Jin, S. J. Moon, J.-Y. Kim, B.-G. Park, C. S. Leem, J. Yu, T. W. Noh, C. Kim, S.-J. Oh, J.-H. Park, V. Durairaj, G. Cao, and E. Rotenberg, Phys. Rev. Lett. **101**, 076402 (2008).
[6] B. J. Kim, H. Ohsumi, T. Komesu, S. Sakai, T. Morita, H. Takagi, and T. Arima, Science **323**, 1329 (2009).
[7] Y. K. Kim, O. Krupin, J. D. Denlinger, A. Bostwick, E. Rotenberg, Q. Zhao, J. F. Mitchell, J. W. Allen, and B. J. Kim, Science **345**, 187 (2014).
[8] Y. K. Kim, N. H. Sung, J. D. Denlinger, and B. J. Kim, Nat. Phys. **12**, 37 (2016).
[9] S. N. Ruddlesden and P. Popper, Acta Crystallogr. **11**, 54 (1958).
[10] S. J. Moon, H. Jin, K. W. Kim, W. S. Choi, Y. S. Lee, J. Yu, G. Cao, A. Sumi, H. Funakubo, C. Bernhard, and T. W. Noh, Phys. Rev. Lett. **101**, 226402 (2008).
[11] J. W. Kim, Y. Choi, J. Kim, J. F. Mitchell, G. Jackeli, M. Daghofer, J. van den Brink, G. Khaliullin, and B. J. Kim, Phys. Rev. Lett. **109**, 037204 (2012).
[12] J. G. Zhao, L. X. Yang, Y. Yu, F. Y. Li, R. C. Yu, Z. Fang, L. C. Chen, and C. Q. Jin, J. Appl. Phys. **103**, 103706 (2008).
[13] J. Matsuno, K. Ihara, S. Yamamura, H. Wadati, K. Ishii, V. V. Shankar, H.-Y. Kee, and H. Takagi, Phys. Rev. Lett. **114**, 247209 (2015).
[14] L. Hao, D. Meyers, C. Frederick, G. Fabbris, J. Yang, N. Traynor, L. Horak, D. Kriegner, Y. Choi, J.-W. Kim, D. Haskel, P. J. Ryan, M. P. M. Dean, and J. Liu, Phys. Rev. Lett. **119**, 027204 (2017).
[15] J. M. Longo, J. A. Kafalas, and R. J. Arnott, J. Solid State Chem. **3**, 174 (1971).
[16] Y. F. Nie, P. D. C. King, C. H. Kim, M. Uchida, H. I. Wei, B. D. Faeth, J. P. Ruf, J. P. C. Ruff, L. Xie, X. Pan, C. J. Fennie, D. G. Schlom, and K. M. Shen, Phys. Rev. Lett. **114**, 016401 (2015).
[17] See Supplemental Material at http://link.aps.org/supplemental/10.1103/PhysRevLett.119.256404 for detailed information on sample growth, structural characterizations, experimental data, and theoretical calculations, which includes Refs. [18–25].
[18] S. R. Foltyn, R. C. Dye, K. C. Ott, E. Peterson, K. M. Hubbard, W. Hutchinson, R. E. Muenchausen, R. C. Estler, and X. D. Wu, Appl. Phys. Lett. **59**, 594 (1991).
[19] G. Rijnders, D. H. A. Blank, J. Choi, and C.-B. Eom, Appl. Phys. Lett. **84**, 505 (2004).
[20] E. H. P. Cordfunke and G. Meyer, Recl. Trav. Chim. **81**, 495 (1962).
[21] K. Nishio, H. Y. Hwang, and Y. Hikita, APL Mater. **4**, 036102 (2016).
[22] D. I. Woodward and I. M. Reaney, Acta Crystallogr. Sect. B **61**, 387 (2005).
[23] J.-M. Carter, V. V. Shankar, M. A. Zeb, and H.-Y. Kee, Phys. Rev. B **85**, 115105 (2012).
[24] M. A. Zeb and H.-Y. Kee, Phys. Rev. B **86**, 085149 (2012).
[25] J. Liu, D. Kriegner, L. Horak, D. Puggioni, C. Rayan Serrao, R. Chen, D. Yi, C. Frontera, V. Holy, A. Vishwanath, J. M. Rondinelli, X. Marti, and R. Ramesh, Phys. Rev. B **93**, 085118 (2016).
[26] V. N. Strocov, T. Schmitt, U. Flechsig, T. Schmidt, A. Imhof, Q. Chen, J. Raabe, R. Betemps, D. Zimoch, J. Krempasky, X. Wang, M. Grioni, A. Piazzalunga, and L. Patthey, J. Synchrotron Radiat. **17**, 631 (2010).
[27] V. N. Strocov, X. Wang, M. Shi, M. Kobayashi, J. Krempasky, C. Hess, T. Schmitt, and L. Patthey, J. Synchrotron Radiat. **21**, 32 (2013).

[28] G. Kresse and J. Furthmüller, Phys. Rev. B **54**, 11169 (1996).
[29] P. E. Blöchl, Phys. Rev. B **50**, 17953 (1994).
[30] G. Kresse and D. Joubert, Phys. Rev. B **59**, 1758 (1999).
[31] J. P. Perdew, K. Burke, and M. Ernzerhof, Phys. Rev. Lett. **77**, 3865 (1996).
[32] S. Steiner, S. Khmelevskyi, M. Marsmann, and G. Kresse, Phys. Rev. B **93**, 224425 (2016).
[33] A. I. Liechtenstein, V. I. Anisimov, and J. Zaanen, Phys. Rev. B **52**, R5467 (1995).
[34] K. Momma and F. Izumi, J. Appl. Crystallogr. **44**, 1272 (2011).
[35] H. Zhang, K. Haule, and D. Vanderbilt, Phys. Rev. Lett. **111**, 246402 (2013).
[36] B. Kim, P. Liu, and C. Franchini, Phys. Rev. B **95**, 115111 (2017).
[37] R. Arita, J. Kuneš, A. V. Kozhevnikov, A. G. Eguiluz, and M. Imada, Phys. Rev. Lett. **108**, 086403 (2012).
[38] C. Martins, M. Aichhorn, L. Vaugier, and S. Biermann, Phys. Rev. Lett. **107**, 266404 (2011).
[39] W. Ku, T. Berlijn, and C.-C. Lee, Phys. Rev. Lett. **104**, 216401 (2010).
[40] Z. T. Liu, M. Y. Li, Q. F. Li, J. S. Liu, W. Li, H. F. Yang, Q. Yao, C. C. Fan, X. G. Wan, Z. Wang, and D. W. Shen, Sci. Rep. **6**, 30309 (2016).
[41] A. Yamasaki, H. Fujiwara, S. Tachibana, D. Iwasaki, Y. Higashino, C. Yoshimi, K. Nakagawa, Y. Nakatani, K. Yamagami, H. Aratani, O. Kirilmaz, M. Sing, R. Claessen, H. Watanabe, T. Shirakawa, S. Yunoki, A. Naitoh, K. Takase, J. Matsuno, H. Takagi, A. Sekiyama, and Y. Saitoh, Phys. Rev. B **94**, 115103 (2016).
[42] Recently, a Dirac-like feature in the band structure of $SrIrO_3$ has been discussed in the literature. For more details related to our present work, see Supplemental Material, Sec. VIII.
[43] D. J. Groenendijk, C. Autieri, J. Girovsky, M. Carmen Martinez-Velarte, N. Manca, G. Mattoni, A. M. R. V. L. Monteiro, N. Gauquelin, A. F. Otte, M. Gabay, S. Picozzi, and A. D. Caviglia, preceding Letter, Phys. Rev. Lett. **119**, 256403 (2017).
[44] M. K. Crawford, M. A. Subramanian, R. L. Harlow, J. A. Fernandez-Baca, Z. R. Wang, and D. C. Johnston, Phys. Rev. B **49**, 9198 (1994).
[45] M. A. Subramanian, M. K. Crawford, and R. L. Harlow, Mater. Res. Bull. **29**, 645 (1994).
[46] G. Cao, Y. Xin, C. S. Alexander, J. E. Crow, P. Schlottmann, M. K. Crawford, R. L. Harlow, and W. Marshall, Phys. Rev. B **66**, 214412 (2002).
[47] S. Boseggia, R. Springell, H. C. Walker, A. T. Boothroyd, D. Prabhakaran, D. Wermeille, L. Bouchenoire, S. P. Collins, and D. F. McMorrow, Phys. Rev. B **85**, 184432 (2012).
[48] S. Boseggia, H. C. Walker, J. Vale, R. Springell, Z. Feng, R. S. Perry, M. M. Sala, H. M. Rønnow, S. P. Collins, and D. F. McMorrow, J. Phys. Condens. Matter **25**, 422202 (2013).
[49] J.-M. Carter, V. Shankar V., and H.-Y. Kee, Phys. Rev. B **88**, 035111 (2013).
[50] D. J. Groenendijk, N. Manca, G. Mattoni, L. Kootstra, S. Gariglio, Y. Huang, E. van Heumen, and A. D. Caviglia, Appl. Phys. Lett. **109**, 041906 (2016).
[51] G. Shirane and Y. Yamada, Phys. Rev. **177**, 858 (1969).
[52] A. M. Glazer, Acta Crystallogr. Sect. B **28**, 3384 (1972).